X-ray diffraction of heavy-atom labelled two-dimensional crystals of rhodopsin identifies the position of cysteine 140 in helix 3 and cysteine 316 in helix 8

ARTICLE *in* JOURNAL OF MOLECULAR BIOLOGY · MARCH 2002

Impact Factor: 4.33 · DOI: 10.1006/jmbi.2001.5352 · Source: PubMed

5 AUTHORS, INCLUDING:

Thorsten Mielke
Max Planck Institute for Molecular Genetics
54 PUBLICATIONS **2,664** CITATIONS
SEE PROFILE

Gebhard F X Schertler
Paul Scherrer Institut
88 PUBLICATIONS **8,196** CITATIONS
SEE PROFILE

Maarten P Heyn
Freie Universität Berlin
119 PUBLICATIONS **4,921** CITATIONS
SEE PROFILE

doi:10.1006/jmbi.2001.5352 available online at http://www.idealibrary.com on IDEAL® J. Mol. Biol. (2002) 316, 693–709

JMB

X-ray Diffraction of Heavy-atom Labelled Two-dimensional Crystals of Rhodopsin Identifies the Position of Cysteine 140 in Helix 3 and Cysteine 316 in Helix 8

Thorsten Mielke[1], Claudio Villa[2], Patricia C. Edwards[2] Gebhard F. X. Schertler[2]* and Maarten P. Heyn[1]*

[1]*Biophysics Group, Department of Physics, Freie Universität Berlin, Arnimallee 14 D-14195 Berlin, Germany*

[2]*Medical Research Council Laboratory of Molecular Biology, Hills Road, Cambridge CB2 2QH, UK*

We have used site-specific heavy-atom labelling and X-ray diffraction to localize single amino acid residues in the cytoplasmic domain of the integral membrane protein rhodopsin, the dim-light photoreceptor of retinal vertebrate rod cells. Two-dimensional orthorhombic crystals of the space group $p22_12_1$ ($a = 59.5(\pm1)$ Å and $b = 82.7(\pm1.5)$ Å) were produced from detergent-solubilized, partially delipidated rhodopsin. To obtain milligram amounts of two-dimensional crystals, which are required for X-ray diffraction, the yield of the crystalline material was significantly increased by reconstitution of rhodopsin in the presence of cholesterol (1:2 to 1:10 mol/mol) and by adding polar organic solvents to the dialysis buffer. The native cysteine residues C140 and C316 were then selectively labelled with mercury using the sulphydryl-specific reagent *p*-chloromercuribenzoate (1.6-2.1 mol Hg per mol rhodopsin). The labelling did not affect the unit cell dimensions. Optical absorption spectra of labelled and native two-dimensional rhodopsin crystals showed the characteristic 11-*cis*-retinal peak at 498 nm, which corresponds to the dark state of rhodopsin. The in-plane position of the mercury label was calculated at 9.5 Å resolution from the intensity differences in the X-ray diffraction patterns of labelled and native crystals using Fourier difference methods and the phase information from electron crystallography. The label positions were in excellent agreement with the positions of C140 at the cytoplasmic end of helix 3 and of C316 in the cytoplasmic helix 8 recently obtained from three-dimensional rhodopsin crystals. Whereas these high-resolution diffraction studies were performed under cryogenic conditions (100 K), our results were obtained at room temperature with fully hydrated membranes and in the absence of loop-loop crystal contacts. To study the structural changes of the cytoplasmic loops involved in activation and signal transduction, our more physiological conditions offer important advantages. Furthermore, the localization of C316 is the first direct proof that the electron density on top of helix 1 observed by cryo-electron microscopy is a part of the C-terminal loop. Our approach is of particular interest for investigations of other membrane proteins, for which 3D crystals are not available. Structural constraints from heavy-atom labels at strategic sites enable the assignment of a position in the amino acid sequence to features visible in a low-resolution density map and the study of conformational changes associated with different functional states of the membrane protein.

Present address: T. Mielke, Medical Research Council, Laboratory of Molecular Biology, Hills Road, Cambridge CB2 2QH, United Kingdom.

Abbreviations used: CTF, contrast transfer function; DMSO, dimethylsulphoxide; DTT, dithiothreitol; LDAO, lauryldimethylamine oxide; MPD, 2-methyl-2,4-pentandiol; PCMB, *p*-chloromercuribenzoate.

E-mail addresses of the corresponding authors: heyn@physik.fu-berlin.de; gfx@mrc-lmb.cam.ac.uk

0022-2836/02/030693–17 $35.00/0

*Corresponding authors

Keywords: rhodopsin; two-dimensional crystals; membrane proteins; X-ray diffraction; heavy-atom labelling

Introduction

The number of high-resolution membrane protein structures solved by X-ray crystallography is still low because of the general difficulties in growing well-ordered three-dimensional (3D) crystals. Since two-dimensional (2D) crystals of membrane proteins are often easier to obtain, electron crystallography has become an important alternative technique to determine the structure of these biologically extremely important molecules.[1–3] In favourable cases, atomic resolution comparable to X-ray crystallography was achieved.[4–7] In addition, a wide range of low-resolution structures of membrane proteins have been obtained including rhodopsin,[8,9] halorhodopsin[10] and different ATPases.[11,12] However, interpretation of low-resolution electron density maps is sometimes difficult. In a number of cases, a clear assignment of hydrophobic stretches from helices in the amino acid sequence to density features representing helices in a low-resolution electron density map was not possible.[13–18]

Rhodopsin, the dim-light photoreceptor of vertebrate retinal rod cells, is a prototypical G protein-coupled receptor. G protein-coupled receptors are central elements of eukaryotic signal transduction. Different members of the family respond to a wide range of extracellular stimuli including neurotransmitters, hormones, odorants and different colours of light. Upon activation, a conformational change at the cytoplasmic surface of the receptor triggers a signal transduction cascade.[19–21] By analogy to other G protein-coupled receptors, the 11-*cis* retinal chromophore of rhodopsin, which is covalently bound as a protonated Schiff base to K296, serves as an antagonist in the dark state. Upon photo-isomerization to the all-*trans* isomer, rhodopsin is converted through a series of spectroscopically distinguishable intermediates to metarhodopsin II, which corresponds to the agonist state and activates the heterotrimeric G protein transducin.[22–24]

The first low-resolution structures of a G protein-coupled receptor were obtained by electron crystallography of 2D rhodopsin crystals.[8,9,25,26] A combination of these low-resolution structures and structural constraints from amino acid sequence analysis of several hundred G protein-coupled receptors was used to obtain an α-carbon template for the transmembrane domain in the receptor family.[27] Furthermore, some electron density was observed at the extracellular side of the rhodopsin molecule, which was interpreted as part of the extracellular domain comprising the N-terminal tail and the loops connecting the transmembrane helices.[8] The cytoplasmic domain appeared to be less structured. Some density was observed for the loop connecting helix 1 and helix 2. An additional density peak was found close to the top of helix 1, which was interpreted as an ordered part of the C-terminal tail.[8,28]

Recently well-ordered 3D crystals of bovine rhodopsin were obtained from mixed detergent micelles[29] and a model of rhodopsin was derived from X-ray diffraction data extending to 2.8 Å resolution.[30] These data confirmed the presence of a highly organized extracellular domain. High crystallographic temperature factors observed for the cytoplasmic loop domain and the lack of several amino acid residues from the C3-loop and the C-terminal tail indicate that this part of the receptor is less structured. The most striking feature of the cytoplasmic surface is the presence of another helical structure (helix 8) connecting helix 7 and the C-terminal palmitoylation sites.

Here, we have localized single amino acid residues on the surface of rhodopsin by site-directed heavy-atom labelling using 2D crystals, which were produced by reconstitution of detergent-solubilized rhodopsin. In the crystal, the native cysteine residues C140 and C316 were derivatised using *p*-chloromercuribenzoate (PCMB). The positions of the mercury atoms were then determined from X-ray powder diffraction patterns of multilamellar films of 2D crystals by Fourier difference techniques using the phase information from electron crystallography.[31] The positions were in excellent agreement with both the α-carbon template of the transmembrane domain of G protein-coupled receptors[27] and the high-resolution crystal structure of rhodopsin.[30] These are the first results from X-ray diffraction with 2D crystals of rhodopsin. Since they are obtained at room temperature with fully hydrated membrane samples, in which intermolecular loop-loop contacts are minimal, this method provides complementary structural information under more native experimental conditions. Our approach is also very attractive for investigations of other integral membrane proteins, for which low-resolution structures derived from 2D crystals are available.

Results

2D-crystallisation of bovine rhodopsin

The X-ray approach described here requires homogeneous crystalline material in milligram amounts. To obtain the desired amount of 2D rhodopsin crystals, previous crystallisation procedures[9] needed to be scaled-up. For this purpose we have tested different modifications of the reconstitution and dialysis conditions as described in Material and Methods. Variations of the

temperature, pH and salt composition of the dialysis buffer did not improve the sample quality (data not shown). Increasing the concentration of reducing agents such as DTT or mercaptoethanol in the dialysis buffer improved the formation of crystals significantly. However, better crystalline samples were obtained when a combination of 4 mM DTT and 4 mM mercaptoethanol was used. The yield of crystalline material *versus* non-crystalline protein aggregates was further improved by addition of organic solvents to the dialysis buffer as indicated by low magnification pictures of negative stained samples (Figure 1). After dialysis in the presence of 2.5 % (v/v) isopropanol or 2.5 % (v/v) 2-methyl-2,4-pentanediol (MPD), preparations showed mainly crystalline material and only minor traces of aggregates. A similar but weaker effect was observed after the addition of DMSO (data not

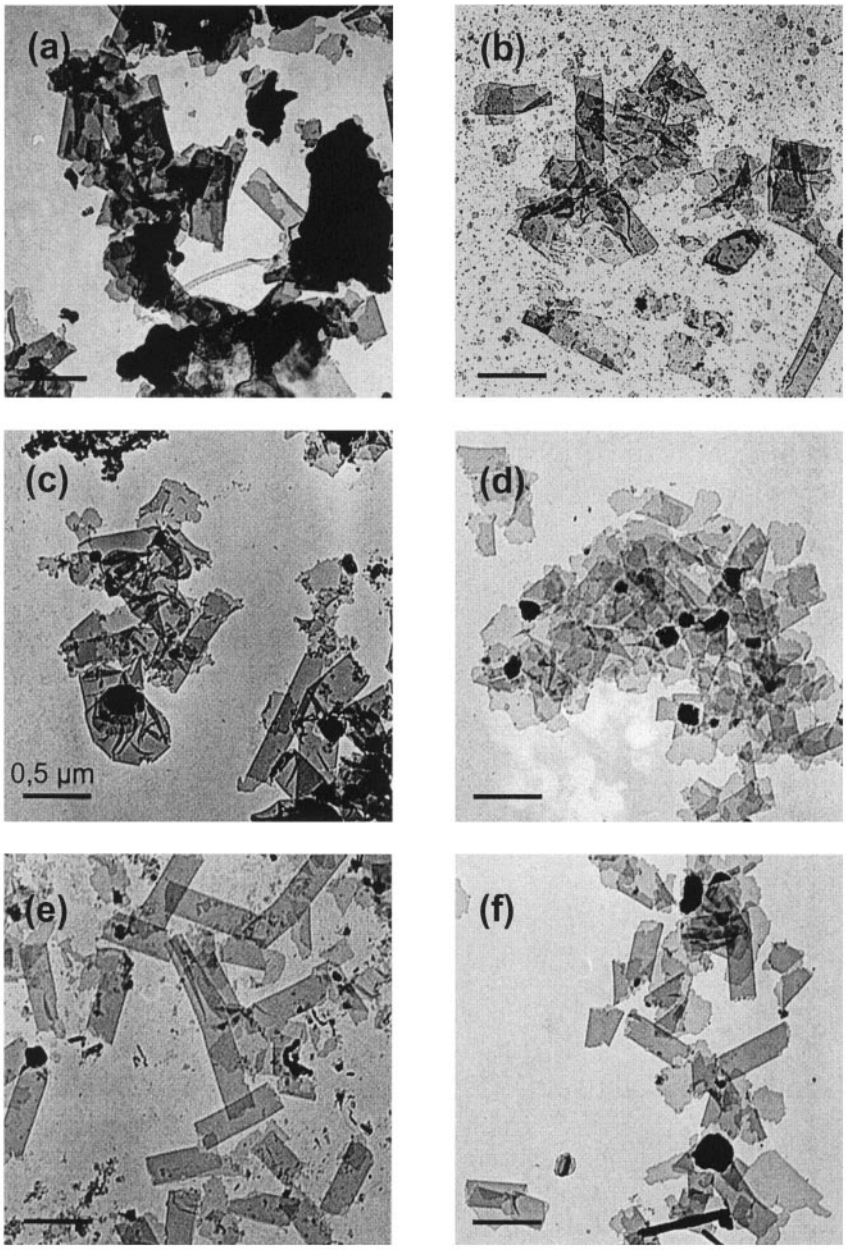

Figure 1. Representative low magnification electron micrographs of negative stained rhodopsin 2D crystals. Crystals were obtained by dialysis against a buffer containing 20 mM Hepes, 100 mM NaCl, 10 mM $MgCl_2$, 3 mM NaN_3 (pH 7.0). Additionally 1 mM DTT (a), 4 mM DTT and 4 mM mercaptoethanol (b), 2 mM DTT (c), 4 mM DTT, 4 mM mercaptoethanol and 2.5 % (v/v) MPD (d), 4 mM DTT, 4 mM mercaptoethanol and 2.5 % (v/v) isopropanol (e) were added to the dialysis buffer. In the experiments (c)-(f) rhodopsin was incubated with 2 mol cholesterol per mol rhodopsin prior to the dialysis. Crystals shown in (f) are from the same sample as shown in (e), but after heavy-atom labelling with PCMB. The scale bars represent 0.5 µm.

shown). It should be noted that the low magnification images in Figure 1 were chosen to represent the average sample quality.

The reconstitution of rhodopsin in the presence of lipids was also investigated. Reconstitution in the presence of native lipids extracted from ROS membranes led mainly to the formation of protein-lipid-vesicles, even at small molar ratios (e.g. 5 mol lipid per mol rhodopsin). Similar results were obtained after reconstitution of rhodopsin in the presence of exogenous lipids (e.g. soy bean phosphatidylcholine and phosphatidylethanolamine, respectively; data not shown). In contrast to these observations, reconstitution of rhodopsin in the presence of cholesterol (e.g. 2:1 mol cholesterol per mol rhodopsin) improved the crystal formation and decreased the amount of aggregated protein significantly. Furthermore, the use of cholesterol also increased the reproducibility of the crystallisation experiments.

In general, crystalline preparations showed predominantly tubular crystals and fewer single layers. Tubes typically showed a diameter of 0.2 μm and a variable length between 1 and 5 μm. The diameter of the single layers varied between 0.2 and 0.5 μm. However, no significant correlation between dialysis conditions and the ratio of tubes to single layers could be observed. An absorption spectrum of a crystalline sample is shown in Figure 2(a). The peak at 498 nm demonstrates the 11-*cis*-conformation of the retinal chromophore, which is characteristic for the ground state of rhodopsin.

Heavy-atom labelling

The mercury-containing reagent PCMB reacts specifically with the sulphydryl group of cysteine residues to form a mercaptide (Figure 2(b)).[32] The formation of the mercaptide is accompanied by an absorption change in the ultraviolet region. The maximum of the difference spectrum between the mercaptide and the unbound PCMB is at 250 nm ($\Delta\varepsilon = 7.600\ M^{-1}$).[33] Thus, the time-course of the labelling reaction was monitored at this wavelength. The cysteine mercaptide has its maximal absorption at 240 nm. Therefore the absorbance difference at 240 nm was used to calculate the labelling stoichiometry after removal of excess of unbound label. After a reaction time of six hours, a labelling stoichiometry of typically 1.6-2.1 mol mercaptide per mol rhodopsin was achieved, indicating the derivatization of two cysteine residues. Figure 2(a) shows an absorption spectrum of rhodopsin crystals before and after labelling. In this experiment, a labelling stoichiometry of 1.65 mol mercaptide per mol rhodopsin was determined from the absorbance difference of 196 m*A* at 240 nm (Figure 2(b)). Within a reaction time of six hours no significant changes in the absorption bands of the retinal chromophore could be observed (see Figure 2(a)).

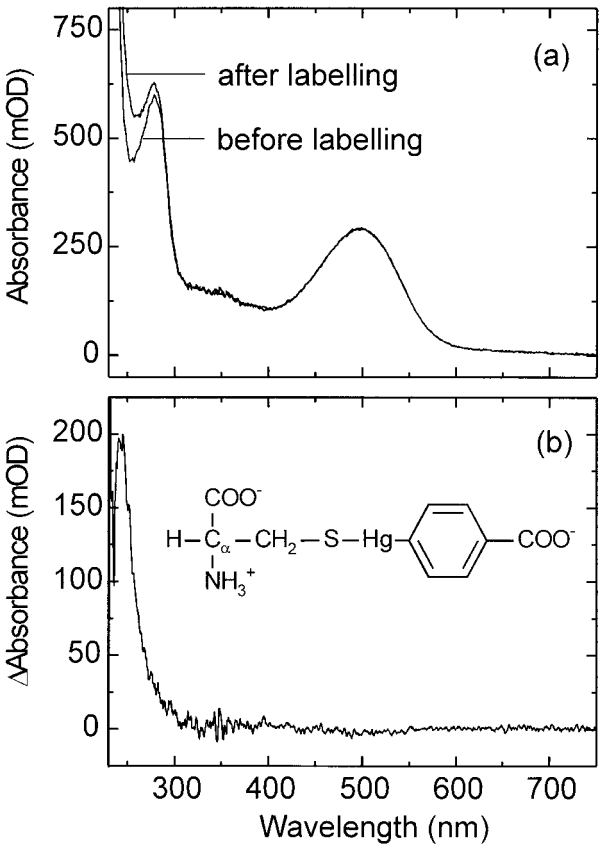

Figure 2. Absorption spectra of rhodopsin 2D crystals before and after labelling with PCMB (a). The labelling reaction was performed with a ten-fold molar excess of PCMB in 1 mM sodium phosphate buffer, 20 mM NaCl (pH 7.0) at room temperature. The reaction time was six hours. The difference spectrum (b) was used to calculate the labelling stoichiometry (1.65 mol mercuribenzoate per mol rhodopsin). Crystals used in this experiment were obtained by reconstitution of rhodopsin in the presence of 10:1 (mol/mol) cholesterol per rhodopsin and dialysis against buffer containing the additives 4 mM DTT, 4 mM mercaptoethanol and 2.5 % (v/v) MPD. The inset in (b) shows the mercuribenzoate bound to cysteine.

Cryo-electron microscopy

2D crystals obtained from different crystallisation exeperiments were analysed by high-resolution cryo-electron microscopy. The lattice parameters showed no significant changes due to the modifications of the dialysis conditions. Lattice constants determined for crystals from different preparations varied between $a = 59.1$-62.4 Å and $b = 83.2$-90.7 Å. The ratio b/a showed a more constant value of 1.42(±0.03) (standard deviation of 43 images). The average angle γ between a and b was 90.0(±0.4) degrees (Table 1). A representation of the Fourier components of a single crystal is shown in Figure 3. To estimate the quality of a single crystal, average peak intensities were calculated for different resolution ranges (infinity to

Table 1. Comparison of images of single crystals taken from different crystalline preparations

Dialysis conditions[a]		2 mM DTT	4 mM DTT 4 mM MeSH[c]	2 mM DTT	4 mM DTT 4 mM MeSH	4 mM DTT, 4 mM MeSH, 2.5 % (v/v) MPD	4 mM DTT, 4 mM MeSH, 2.5 % (v/v) isopropanol	4 mM DTT, 4 mM MeSH, 2.5 % (v/v) isopropanol
Ratio cholesterol/rhodopsin[b]		-	-	2:1	2:1	2:1	2:1	2:1
Mercuribenzoate/rhodopsin[b]		-	-	-	-	-	-	1.9
Image-no.		18,541	93,812	17,461	17,332	24,231	24,501	26,241
a (Å)		59.5	62.1	59.8	61.8	62.1	61.0	61.8
b (Å)		84.9	89.8	84.6	88.9	89.8	86.9	87.9
Ratio *b*/*a*		1.43	1.45	1.42	1.44	1.45	1.43	1.42
γ (°)		89.82	90.05	89.31	90.36	89.84	89.43	89.71
Resolution range ∞-9 Å	Average intensities	893	806	975	1604	237	492	565
	No. of spots	90	88	92	95	80	80	85
	No. of spots *IQ* 1-4	85	85	80	91	69	74	72
Resolution range 9-5 Å	Average intensities	26	22	30	77	19	21	19
	No. of spots	93	89	105	138	63	61	90
	No. of spots *IQ* 1-4	43	43	60	91	28	28	35
Resolution range 5-3.5 Å	Average intensities	9	7	7	14	9	9	9
	No. of spots	61	55	55	100	71	52	79
	No. of spots *IQ* 1-4	8	8	11	38	12	5	19

[a] Substances added to dialysis buffer (20 mM Hepes (pH 7.0), 100 mM NaCl, 10 mM $MgCl_2$, 3 mM NaN_3).
[b] (mol/mol).

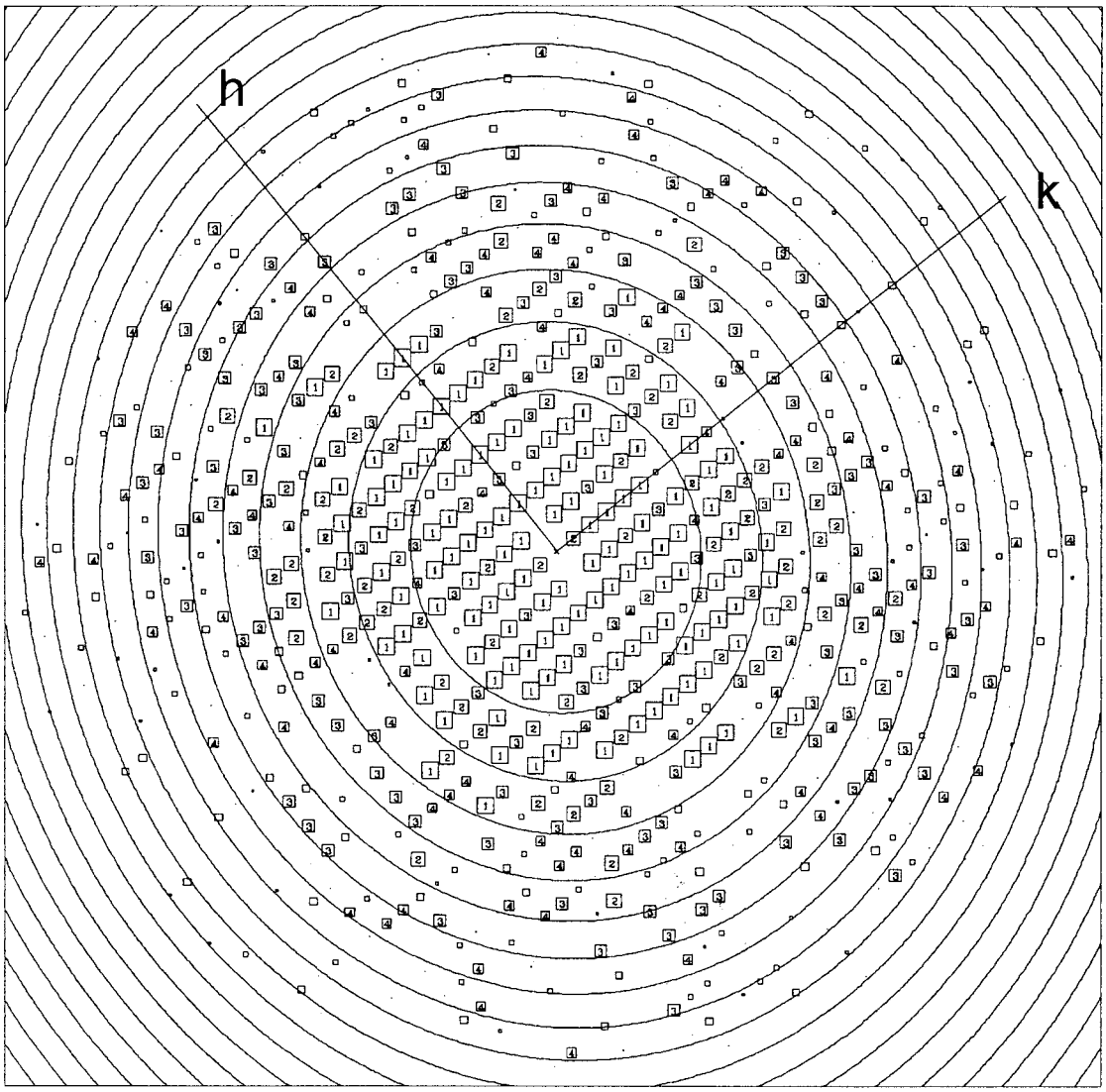

Figure 3. Fourier components of a single image (image no. 17,332) after three rounds of lattice unbending. Each spot is represented by a square with a size proportional to its *IQ* value as described by Henderson *et al.*[63] The numbers of *IQ* values from 1-4 are printed. The continuous circles indicate the zeros of the contrast transfer function. Applied defocus values are $F_x = 5600$ Å and $F_y = 6890$ Å, $\phi = 78°$. This image showed significant information on the periodic structure to 3.5 Å resolution as indicated by the averaged peak intensity value of 14 in the resolution range from 5 to 3.5 Å (Table 1).

9 Å, 9 to 5 Å and 5 to 3.5 Å) and normalized to a background value of 7 (program MMBOXA). An average intensity above the background value of 7 indicates that the image contains useful information on the periodic structure in the selected resolution range. Table 1 shows the results of this analysis for individual crystals, which were performed under different dialysis conditions. All images showed a significant signal above the background in the resolution range of 9 to 5 Å. Nearly every second image contained useful structural information in the resolution range of 5 to 3.5 Å. After CTF refinement, an unsymmetrized projection map (p1 map) was calculated from each single crystal. The untilted helices 4, 6 and 7 were clearly visible in p1 maps of the best images. Inspection of the p1 maps and determination of the plane group (program ALLSPACE) demonstrated that all crystals analysed belonged to the plane group $p22_12_1$. Thus none of the modifications of the dialysis conditions led to the formation of a different crystal form. More importantly, no significant changes of either lattice parameters or crystal quality could be observed by electron microscopy after heavy-atom labelling. These results confirmed that the labelling was isomorphous, which is required for Fourier difference methods. A reference data set was calculated by combining information from four images. Amplitudes were corrected for the resolution-dependent attenuation as described.[9] The projection density map calculated to a resolution of 7 Å showed the typical structural features of bovine

rhodopsin visible at low-resolution (Figure 4). Three strong density peaks perpendicular to the membrane plane represent the least tilted helices 4, 6 and 7. The arc-shaped feature is formed by the more tilted helices 1, 2, 3 and 5.[9]

X-ray diffraction experiments

Multilamellar films of 2D crystals were prepared by drying a concentrated crystal suspension (0.7-1 mg rhodopsin in 1 mM sodium phosphate buffer (pH 7.0), 0-20 mM NaCl) on a Trespaphan support film under constant humidity. However, individual samples obtained from identical dialysis conditions behaved slightly differently during film formation. Therefore the conditions for film formation had to be chosen carefully for each experiment. Best results have been achieved with samples obtained by reconstitution of rhodopsin in the presence of cholesterol (2-10 mol cholesterol per mol rhodopsin) and dialysis against a buffer containing additionally 4 mM mercaptoethanol, 4 mM DTT and 2.5 % (v/v) isopropanol or 2.5 % (v/v) MPD.

To further increase the homogeneity of the crystalline material, samples were purified on a sucrose density gradient (30-50 % (w/v) sucrose). Crystals were harvested from a fraction with a density of 1.2 g/ml. Although purified crystals showed less aggregated material as indicated by low magnification pictures of negative stained samples (data not shown), no stable multilamellar films could be obtained after purification. Even though the crystals were excessively washed in buffer (1 mM sodium phosphate (pH 7.0), 0-20 mM NaCl) to remove the sucrose, drying of these samples led to flat films, which did not adhere to the support film. In a similar way attempts to obtain ordered films from samples containing predominantly protein-lipid-vesicles (e.g. samples obtained by reconstitution of rhodopsin in the presence of ROS lipids) failed. Therefore these samples could not be characterized by X-ray diffraction.

Although samples were kept at constant humidity during film formation and X-ray measurements, only in a few experiments could sample films be stabilized for a time sufficient to collect diffraction data with an adequate signal-to-noise ratio (at least 15-20 hours). Therefore the data collection was performed in one hour runs. Individual runs were checked for systematic errors due to the quality of the sample films and then summed to give one diffraction pattern. Figure 5 shows the X-ray diffraction intensities of a PCMB-labelled and unlabelled rhodopsin sample after background subtraction as a function of the length of the scattering vector $S = 2 \sin \theta/\lambda$. For each sample, 25 individual one hour runs were summed. The crystals used in this experiment were obtained by reconstitution of rhodopsin in the presence of 10:1 (mol/mol) cholesterol per rhodopsin and dialysis against buffer

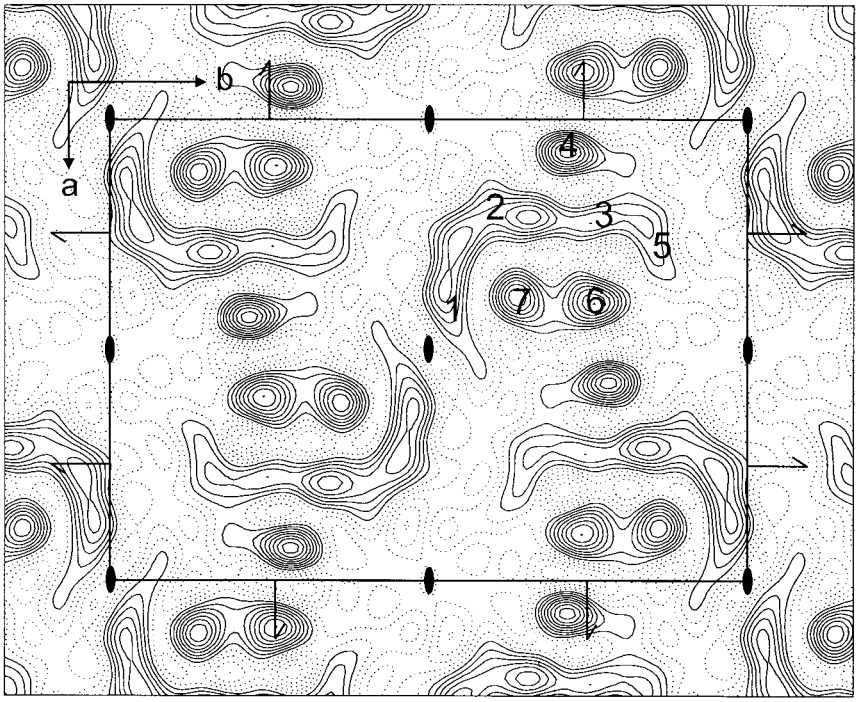

Figure 4. Projection density map of rhodopsin $p22_12_1$ crystals calculated to a resolution of 7 Å using amplitudes and phases from the reference data set obtained from electron microscopy. Unit cell parameters were taken from the X-ray experiment ($a = 59.5$ Å, $b = 82.7$ Å, $\gamma = 90°$). The dotted lines correspond to the density values below zero. The unit cell containing four rhodopsin molecules is represented by the rectangle. The numbers shown in one rhodopsin molecule indicate the positions of the seven transmembrane helices. This molecule is viewed from the cytoplasmic side. The set of 2-fold rotational axes and the sets of 2-fold screw axes along *a* and *b* are shown.

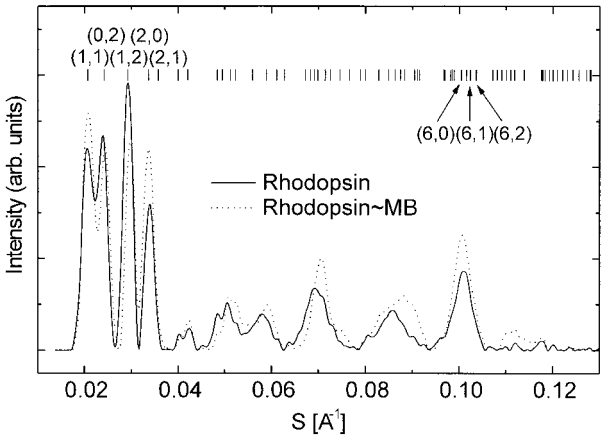

Figure 5. X-ray diffraction intensities of native rhodopsin 2D crystals (continuous line) and PCMB-labelled rhodopsin crystals (dotted line) before Lorentz correction as a function of the length of the scattering vector $S = 2 \sin \theta/\lambda$. The small bars indicate the position of the Bragg reflections calculated for a $p22_12_1$ lattice using the unit cell parameters of $a = 59.5$ Å, $b = 82.7$ Å and $\gamma = 90°$. Some of the reflections which show the highest scattering intensities according to electron microscopy data are labelled with their Bragg indices (h,k).

containing additionally 4 mM mercaptoethanol, 4 mM DTT and 2.5% (v/v) MPD. The sample showed mainly tubular crystals of a length up to 5 μm. The corresponding absorption spectra before and after PCMB-labelling are shown in Figure 2. The unit cell dimensions were determined by fitting a sum of Gaussian distributions to the (1,1), (0,2), (1,2), (2,0), (6,0) and (6,1) reflections, respectively, which have the highest scattering intensities according to electron microscopy data and which are best resolved. The positions of the peaks were modelled according to the equation:

$$S = (h^2/a^2 + k^2/b^2)^{1/2} \quad (1)$$

for an orthorhombic $p22_12_1$ lattice using variable values for the unit cell dimensions a and b. The best overall agreement between the diffraction data from labelled and unlabelled crystals, respectively, and the modelled lattice was obtained with $a = 59.5(\pm1)$ Å and $b = 82.7(\pm1.5)$ Å. Bragg reflections with similar S values according to equation (1) occur at similar Bragg angles and therefore contribute to powder rings (Debye-Scherrer rings) close to each other (none of the reflections occurred under identical Bragg angles). Because of the relatively low signal-to-noise ratio and the rather broad diffraction peaks, Bragg reflections with close S values could not be resolved as single peaks. The intensities of the reflections were determined by fitting a sum of Gaussian distributions to the diffraction data. If necessary, the position of the reflections was set to a fixed value within the error of the experimental unit cell parameters. Intensities from the labelled and unlabelled sample were fitted using identical fit parameters. The intensity of 35 reflections could be determined within the range of $S \leqslant 0.105$ Å^{-1} (Table 2). This corresponds to a resolution of 9.5 Å. Because of the superposition of powder rings from reflections with similar Bragg angles, intensities of eight more reflections with small amplitudes in the direct neighbourhood of strong reflections could not be determined accurately and were neglected. The error of the mathematical intensity fit was less than 5%. However, an additional systematic error due to the background correction cannot be excluded. The intensities were corrected by a Lorentz factor of $(b^2h^2/a^2 + k^2)^{1/2}$. Since the amount of scattering material in the beam can never be the same for the labelled and unlabelled sample, the observed intensities were then normalized such that the sum of the intensities is the same. The overall relative

Table 2. X-ray intensities and structure factor amplitudes of native (Rho) and PCMB-labelled (MB) rhodopsin crystals

h	k	I_{Rho}	I_{MB}	F_{Rho}	F_{MB}	ΔF	h	k	I_{Rho}	I_{MB}	F_{Rho}	F_{MB}	ΔF
1	1	68.3	77.9	8.92	8.50	−0.42	3	4	9.3	16.7	6.05	7.23	1.18
0	2	58.1	55.6	8.89	7.76	−1.13	4	2	6	7.5	4.91	4.90	−0.01
1	2	73.2	54	11.02	8.44	−2.58	1	6	1.3	3.5	2.34	3.42	1.08
2	0	35.8	55	8.23	9.10	0.87	4	3	0.5	1.3	1.47	2.11	0.64
2	1	4.7	5.1	3.08	2.86	−0.22	3	5	1.1	1.3	2.21	2.14	−0.07
1	3	2.3	1.6	2.27	1.69	−0.58	2	6	2.1	2.4	3.08	2.93	−0.15
2	2	4.7	6.5	3.31	3.47	0.16	4	4	4.5	7.7	4.58	5.34	0.76
0	4	5.5	2.7	3.87	2.42	−1.45	5	1	8	9	6.19	5.86	−0.33
2	3	7.8	8.5	4.66	4.34	−0.32	1	7	4.9	4.4	4.89	4.13	−0.76
1	4	6.8	8.6	4.43	4.44	0.01	5	2	2.9	8.5	3.78	5.77	1.99
3	1	3.3	4.8	3.11	3.34	0.23	3	6	3	7.1	3.86	5.30	1.44
3	2	7.2	7.9	4.76	4.45	−0.31	4	5	2.2	5.6	3.35	4.77	1.42
2	4	10.7	14.2	5.96	6.12	0.16	5	3	0.6	4.1	1.75	4.09	2.34
3	3	1.9	2.8	2.58	2.79	0.21	2	7	0.9	2.1	2.15	2.93	0.78
1	5	1.1	0.6	1.97	1.30	−0.67	6	0	15.5	23.4	9.38	10.28	0.90
4	0	6.1	2	4.81	2.45	−2.36	6	1	12.2	17.2	8.36	8.85	0.49
4	1	7.6	2.6	5.41	2.82	−2.59	6	2	6	8.8	5.92	6.39	0.47
2	5	8.3	11	5.69	5.84	0.15							

I_{Rho}, I_{MB}, Intensities of Bragg reflections before Lorentz correction; F_{Rho}, F_{MB}, structure factor amplitudes after normalization; ΔF, resulting differences in structure factor amplitudes representing the label positions.

intensity change $\Sigma|\Delta I|/\Sigma I$ before Lorentz correction was calculated to be 28.4%. In another experiment using the same batch of crystalline material (label stoichiometry 1.7 mol MB per mol rhodopsin), a relative intensity change of 32.0% was observed. The correlation of the corresponding diffraction patterns as judged by the correlation coefficient calculated as described by Glaeser *et al.*[34] was 86.6% indicating a high degree of similarity between both data sets.

The projection structure of native rhodopsin was calculated to 9.5 Å using the amplitudes observed from the X-ray experiment and the phases from the electron microscopy (Figure 6). Four rhodopsin molecules are visible in the unit cell. At this resolution, helices 6 and 7 are not resolved as single density peaks. The weakest density is found for the most tilted helices 3 and 5. However, a very similar projection structure was obtained by limiting the resolution of the reference data set to the same resolution.

The difference density map representing the in-plane positions of the mercury label was calculated using the X-ray difference structure factor amplitudes and the phases from electron microscopy (Figure 7). To interpret this difference map, the first two contour lines of the projection density of native rhodopsin, which was calculated to 7 Å resolution using the reference data set obtained by electron microscopy, are also shown. Merging the reference data set to a resolution beyond 5.5 Å would require beam tilt corrections, which are only reliable with a full 3D data set. With increasing resolution the arc-shaped feature comprising the tilted helices 1, 2, 3 and 5 shows an increasing number of additional density features, which would make Figure 7 difficult to comprehend. Therefore, we have chosen a resolution limit of 7 Å.

The strongest difference density peak (maximum 1) was found close to the position where the cytoplasmic end of helix 3 overlaps with helix 5. We assigned maximum 1 to the position of the mercuribenzoate label bound to C140, which is located at the cytoplasmic end of helix 3.[27,30] The second strongest, sharper peak (maximum 2) showed ~10% less density and was located close to the cytoplasmic end of helix 1, which folds over helix 2. The distance between maximum 2 and the centre of helix 7 was 10 Å. C316 is located in the middle of cytoplasmic helix 8, which folds over helix 1.[30] Therefore we assigned maximum 2 to the mercury label bound to C316. Some weaker difference density (30% less than maximum 1) was found close to helix 4 and outside the boundary of the projection density of the rhodopsin molecule. This extra density is most likely due to the errors in the experimental structure factor amplitudes and the series termination error.

The label positions in the difference density map can be described relative to the origin of the unit

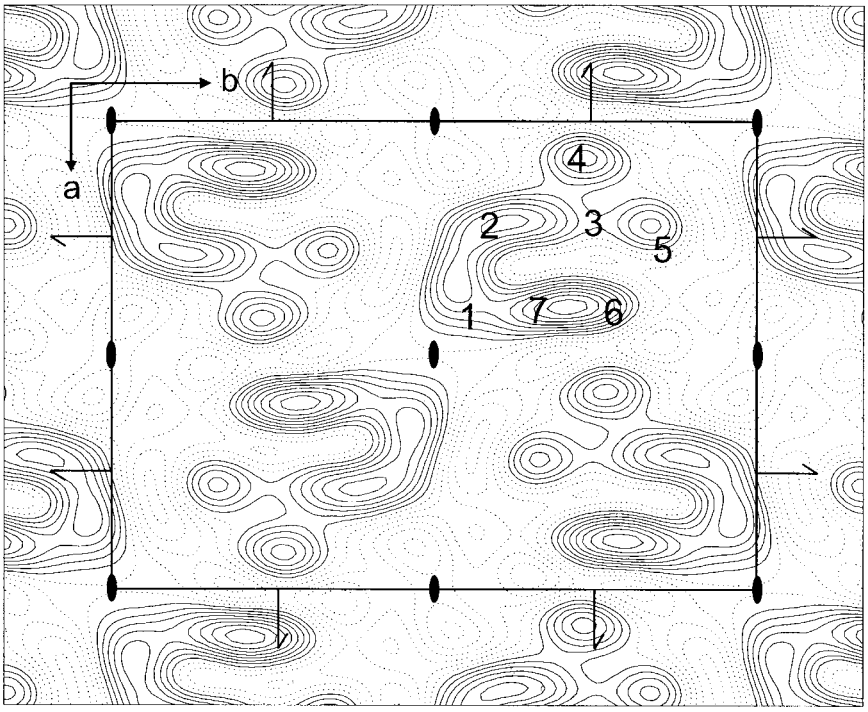

Figure 6. X-ray projection density map of native rhodopsin $p22_12_1$ crystals at 9.5 Å resolution. X-ray intensities of 35 Bragg reflections within the range of $S = 0$-0.105 Å and the corresponding phases from electron crystallography were used to calculate this map. The continuous rectangle represents one unit cell containing four rhodopsin molecules. The lattice parameters are $a = 59.5$ Å, $b = 82.7$ Å and $\gamma = 90°$. The positions of the seven transmembrane helices and the symmetry elements are indicated according to Figure 4.

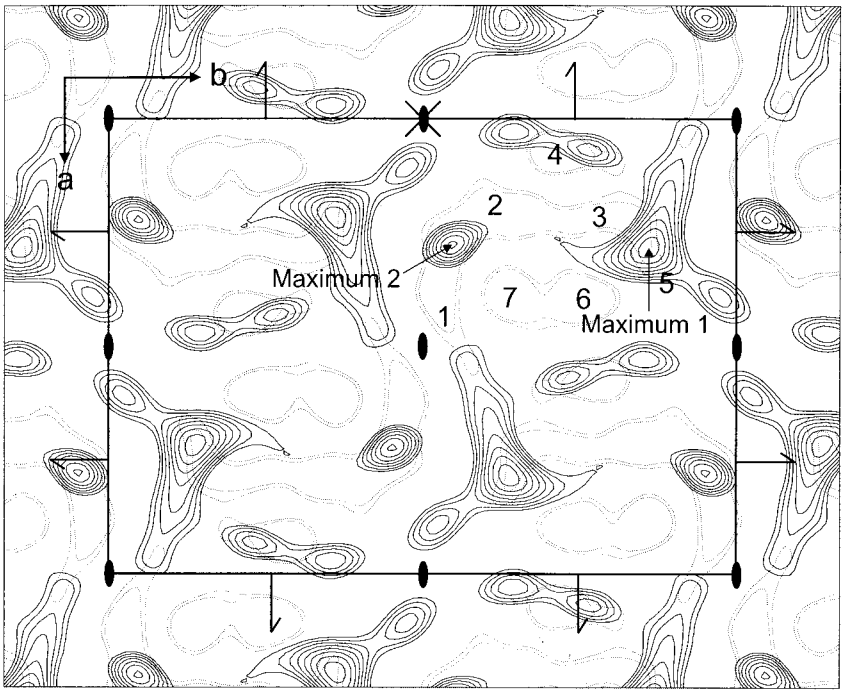

Figure 7. 2D X-ray difference density map showing the positions of the two mercuribenzoate molecules bound to rhodopsin. The contour lines range from 31 to 94 % of the positive difference density in equidistant steps. The two dotted contour lines indicate the boundary of the projection density of native rhodopsin calculated to 7 Å resolution using the reference data set obtained by electron crystallography. The unit cell is marked by the continuous rectangle. Lattice parameters are $a = 59.5$ Å, $b = 82.7$ Å and $\gamma = 90°$. The cross indicates the origin of the unit cell. The set of 2-fold rotational axes and the sets of 2-fold screw axes along a and b are shown. In one rhodopsin molecule, the positions of the transmembrane helices are indicated by the numbers 1-7. This molecule is viewed from the cytoplasmic side. The highest difference densities were found close to the cytoplasmic end of helix 3 (maximum 1) and close to the cytoplasmic end of helix 1 approximately 10 Å away from the centre of helix 7 (maximum 2), respectively. These difference density peaks represent the mercuribenzoate label bound to C140 (maximum 1) and to C316 (maximum 2).

cell using dimensionless fractional coordinates. In these fractional coordinates, the x and y values along the axes of the unit cell are divided by the lengths of the unit cell dimensions ($x \rightarrow x/a$; $y \rightarrow y/b$). The location of the coordinate origin is indicated by the cross in Figure 7. The fractional coordinates obtained from two experiments are summarized in Table 3. Although the resolution of the X-ray experiments was low (9.5 Å), the small differences in the label positions demonstrate the excellent reproducibility of the experiment. The reliability of the label positions was tested by refining the experimental structure factor amplitudes (ΔF values) against a model data set, which consisted of two mercury atoms at different positions in the unit cell. Differences between the experimental and model structure factor amplitudes were minimized by a least square method and variation of the label positions using the Shelx 76 software. The final label positions did not vary significantly if the observed label positions were used as starting points (Table 3). These results support the conclusion that the difference density peaks realistically represent two mercury atoms localized at the observed positions in the unit cell.

Discussion

We have used site-directed heavy-atom labelling in combination with X-ray powder diffraction and Fourier difference techniques to localize the native cysteine residues C140 and C316 in 2D rhodopsin crystals. Both cysteine residues were derivatized with *p*-chloromercuribenzoate. The positions of the mercury atoms were determined from the X-ray intensity differences of labelled and native rhodopsin crystals using the phase information from electron crystallography. The justification of this procedure has been discussed in detail.[31] This approach was recently used successfully to localize single amino acids on the surface of the integral membrane protein bacteriorhodopsin.[33,35] Similar Fourier difference techniques have been used to

Table 3. Fractional coordinates of the observed label positions

Peak	Assignment		Experiment 1[a]	Experiment 2[a]
Maximum 1	C140	x/a	0.286 (0.294)	0.291 (0.255)
		y/b	0.363 (0.369)	0.359 (0.373)
Maximum 2	C316	x/a	0.281 (0.271)	0.286 (0.309)
		y/b	0.044 (0.049)	0.048 (0.019)

[a] The values in brackets represent the fractional coordinates after refining the observed differences in structure factor amplitudes.

investigate the position and orientation of the retinal chromophore in bacteriorhodopsin by neutron diffraction with selectively deuterated retinals[36–38] and the sulphur atom distribution of the native methionine residues using multiple wavelength anomalous diffraction at the sulphur K-edge.[39] While bacteriorhodopsin forms a natural 2D lattice in the purple membrane of *Halobacterium salinarium*, we have now extended this approach to investigate 2D crystals obtained by reconstitution of detergent-solubilized rhodopsin. Due to the orthorhombic $p22_12_1$ symmetry of the rhodopsin crystals, the phase factors are real. Under these conditions the transfer of the phase information from electron crystallography is expected to be an excellent approximation. The X-ray diffraction approach requires milligram amounts of homogeneous crystalline material, whereas only a single 2D crystal suffices for imaging by electron microscopy. Therefore an essential step in this project was to scale-up and optimise the crystallisation procedure to obtain the required amount of crystalline material.

2D crystals of rhodopsin from different organisms were recently produced by either reconstitution of partially delipidated rhodopsin (bovine rhodopsin[9]) or by selective lipid extraction from native photoreceptor membranes (frog rhodopsin[8,40]). We were able to improve the reproducibility of the reconstitution and dialysis conditions to obtain more homogeneous preparations of $p22_12_1$ crystals from 5-10 mg bovine rhodopsin. However, the process of crystal formation depends on many parameters and is not yet completely understood. The effect of a specific modification is thus difficult to interpret.[2,41] We observed a significant improvement of the crystal formation after increasing the concentration of DTT or mercaptoethanol in the buffer of our dialysis system most likely due to the prevention of oxidative events. Interestingly, a mixture of DTT and mercaptoethanol (4 mM each) was found to be optimal. Furthermore, addition of polar organic solvents like isopropanol, MPD and DMSO led to a significant decrease of non-crystalline, aggregated protein. An enhancement of crystal growth in the presence of isopropanol or MPD was observed in crystallisation trials of bacterial cytochrome oxidases[42] or the Na^+/H^+ antiporter from *Escherichia coli* inner membranes.[13]

In reconstitution experiments, the optimisation of the ratio between protein and lipid molecules is crucial for the crystallisation process.[2,41] However, the final mixture between endogenous lipids remaining after protein purification and additional lipids added in reconstitution experiments is difficult to control. Most membrane protein purification techniques (e.g. affinity chromatography) are only partially delipidating. The nature as well as the number of the remaining lipid molecules may differ because of slight variations between each purification experiment and the variability of the lipid composition in biological membranes. In our experiments, reconstitution of rhodopsin even in the presence of small molar ratios between cholesterol and rhodopsin (2:1 to 10:1 mol/mol) significantly improved the formation of $p22_12_1$ crystals, most likely due to the stabilization of rhodopsin by specific lipid-protein interactions. This observation is supported by fluorescence energy transfer measurements between tryptophan sidechains of rhodopsin in ROS membranes containing cholestatrienol, which led to the suggestion of a specific cholesterol-binding site at the hydrophobic lipid-exposed surface of the rhodopsin molecule.[43] Reconstitution of rhodopsin in the presence of native lipids extracted from ROS membranes or exogenous lipids even at small molar lipid to protein ratios (e.g. 5:1 mol/mol) led mainly to the formation of protein-lipid-vesicles. Such vesicles might contain small crystalline areas, which have been analysed successfully by electron crystallography earlier, but the resolution of these studies was limited to 9 Å.[25,26] However, the high amount of polyunsaturated fatty acids typically found in ROS membranes (up to 50 %)[44] raises the question whether other specific lipid-protein interactions occur, which might support the crystallisation of rhodopsin.

Optical absorption spectra taken from rhodopsin 2D crystals suspended in aqueous solution showed the typical retinal peak at 498 nm, which is characteristic for the 11-*cis*-configuration of the protonated retinylidene chromophore in the rhodopsin ground state. The heavy-atom labelling of rhodopsin crystals led to the incorporation of 1.6-2.1 mol mercuribenzoate per mol rhodopsin, indicating the derivatization of two cysteine residues. The achieved high occupancy of the labelling sites is an advantage for determining the label positions. Low occupancy would lead to positional disorder and a reduction in the amplitudes of the Fourier difference peaks, making it more difficult to localize the labels. According to the absorption spectra before and after labelling, under the given labelling conditions no absorption changes in the chromophore region were observed, indicating that, after labelling, rhodopsin is in its ground state conformation. This, together with the unchanged unit cell dimensions, is conclusive evidence that the derivatization of rhodopsin crystals with PCMB is isomorphous. The achieved binding stoichiometry and the reaction profile are in very good agreement with previous studies of the sulphhydryl chemistry in rhodopsin using various sulphhydryl-specific reagents including PCMB.[45–47] These studies revealed that under mild reaction conditions and in the dark only the cysteine residues C140 and C316 are accessible, except when very hydrophobic reagents are used. Since labelling was performed at pH 7, PCMB was charged and not expected to penetrate the membrane. Similar labelling strategies have been used previously to modify C140 and C316 selectively with different spin labels[48] and fluorescent probes.[49]

High-resolution images from crystals embedded in vitrified ice were taken to analyse (I) the unit

cell dimensions, (II) the space group of the lattice and (III) the crystal quality. All images contained periodic information to at least 5 Å resolution, indicating high crystallinity before and after heavy-atom labelling. Crystals showed $p22_12_1$ symmetry in agreement with previous crystallisation experiments.[9] For the X-ray approach described here, the observation of the same unit cell dimensions before and after heavy-atom labelling is essential. Otherwise, the amplitudes of the continuous Fourier transform of the electron density are sampled at different points. Lattice constants observed by X-ray diffraction were at the lower end of the range of the unit cell dimensions obtained by electron microscopy. However, lattice constants determined by electron microscopy in general show a higher uncertainty because of variations of the actual magnification depending on slightly different settings of the microscope for each individual image. Electron diffraction techniques offer promise to achieve more accurate amplitudes compared to electron imaging. However, the difference in scattering power for a heavy-atom is much smaller for electrons than for X-ray radiation. Therefore, locating heavy-atoms by electron diffraction is more difficult compared to X-ray diffraction.[50] Currently, the quality and reproducibility of electron diffraction data from rhodopsin 2D crystals is not sufficient to determine the position of a heavy-atom label.

Crystalline samples were tested for their suitability to form well-ordered multilamellar films. Whereas native crystalline patches of bacteriorhodopsin form stable films when dried from an aqueous suspension[33,35], rhodopsin crystals were more difficult to handle. The reproducibility of the film formation was low. It seems likely that single layers are more suitable to produce well-ordered films. However, in our experiments, the ratio between tubular crystals and single layers did not appear to be correlated with the parameters for optimal film formation. We could remove protein aggregates and small crystal fragments by sucrose density gradient centrifugation, but we could not separate tubular crystals from single layers. However, samples purified on a sucrose gradient did not form stable films.

In comparable X-ray diffraction experiments on better-ordered films of bR crystals a resolution of 7.2 Å was achieved.[33,35] The resolution is dependent on the quality of the crystals and the order of the multilamellar films but other factors are important as well. For example, the Debye-Scherer rings are closer spaced in the $p22_12_1$ rhodopsin crystal than in the $p3$ crystal of bacteriorhodopsin, where Bragg reflections with the same value of $(h^2 + hk + k^2)$ contribute to the same Debye-Scherer ring. Therefore, with increasing resolution it becomes more difficult to extract the amplitudes from overlapping rings. Improved crystals, better-ordered multilamellar films, synchrotron techniques using a very fine beam, and cryo-methods could help to obtain better measurements leading to higher resolution data.

X-ray diffraction patterns of native and PCMB-labelled rhodopsin crystals showed distinct intensity differences due to the presence of the mercury label. The observed differences in structure factor amplitudes of 35 reflections allowed the determination of the label positions. The small differences in the label positions obtained from two different experiments account for the reproducibility and accuracy of the X-ray approach. On the other hand, the observation of two label positions is proof that, in 2D crystals, both labelling sites, C140 and C316, are located in a highly structured environment. Otherwise, the mobility of the binding site would smear out the label density making it difficult or impossible to observe a defined label position.

In the α-carbon model of the transmembrane domain of G protein-coupled receptors, which was based on low-resolution data obtained from 2D rhodopsin crystals, the side-chain of C140 points from helix 3 towards helix 5.[27] According to the 3D X-ray structure of rhodopsin, C140 is located even closer towards the cytoplasmic end of helix 5.[30] A superposition of the observed label positions in projection and these two models is shown in Figure 8(a) and (b), respectively. The maximal distance between the C^{α} atom of the cysteine residue and the mercury atom in the mercaptide is 4.1 Å. In Figure 8, this radius is represented by the circles, which are drawn around the centres of the difference density peaks. The comparison demonstrates that the C^{α} atom of C140, according to both the α-carbon template (Figure 8(a)) and the 3D X-ray structure (Figure 8(b)), fall within the 4.1 Å of maximum 1. Therefore we assigned maximum 1 to the position of the mercuribenzoate bound to C140. Estimating half the resolution of our X-ray experiment (9.5 Å) as the error of the observed label position, Figure 8(b) shows that there is an excellent agreement between our data and the 2.8 Å resolution structure.[30]

We have assigned the second strongest difference density peak (maximum 2) to the mercury label bound to C316, which is located in the fourth cytoplasmic loop connecting helix 7 and the C-terminal palmitoylation sites. From 2D crystals, which resemble the lipid bilayer, the position of C316 was not available at the time the experiments were performed. The position of maximum 2 suggests that in 2D crystals the fourth loop runs from helix 7 towards helix 1 (Figure 8(a)). This result is direct proof that the extra density on top of helix 1 found in a 3D map calculated from tilted 2D crystals of frog rhodopsin[8,28] is indeed a part of the fourth cytoplasmic loop. According to the 3D X-ray structure of rhodopsin, this loop forms a helical structure (helix 8) including the amino acid residues 311 to 321. Helix 8 lies nearly parallel to the cytoplasmic surface and folds over helix 1. C316 is located in the middle of helix 8 and its side-chain points towards the end of helix 1.[30] The

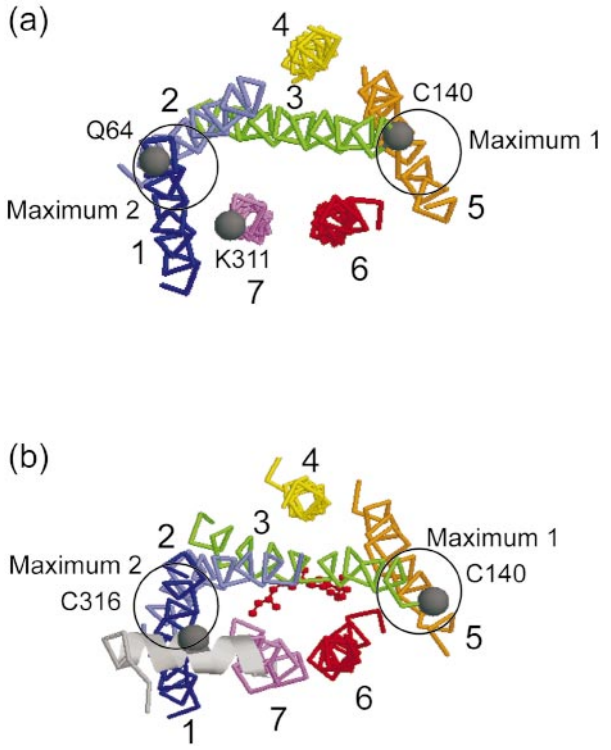

Figure 8. (a) Superposition of the in-plane position of the experimental label positions and the α-carbon template of the transmembrane region of rhodopsin as described by Baldwin *et al*.[27] The rhodopsin molecule is viewed from the cytoplasmic side perpendicular to the membrane plane. The C^{α} atoms of Q64, C140 and K311 located at the cytoplasmic end of helix 1, 3 and 7, respectively, are highlighted. (b) Superposition of the in-plane label positions and the high-resolution 3D model of rhodopsin as described by Palczewski *et al*.[30] For clarity, the extracellular loops and most amino acid residues from the cytoplasmic surface have been removed. The orientation of the rhodopsin molecule is the same as in (a). The C^{α} atoms of C140 and C316 are highlighted. The circles indicate a radius of 4.1 Å around the centre of the difference density peaks and correspond to the maximal distance between the C^{α} atom of the cysteine residue and the bound mercury atom.

C^{α} atom of C316 falls within the 4.1 Å of the difference density maximum 2 (Figure 8(b)). Again, this is an excellent agreement with the 2.8 Å model of rhodopsin.

Whereas C316 is embedded in the well-ordered region of helix 8, helix 3 starts to unwind at the position of C140 at the border to the second cytoplasmic loop. The observed temperature factors also indicate a higher flexibility of C140 compared to C316.[30] These findings are consistent with the broader shape of maximum 1 compared to maximum 2 in our data. Additionally, the lowest contour levels of maximum 1 superimpose with some weaker density outside the boundary of rhodopsin. Figure 7 shows another difference density peak near helix 4, which is more than 30 % smaller than maximum 1. This maximum cannot be due to the label bound to C140, since the distance between the cytoplasmic end of helix 3 and this weaker density is more than 10 Å and thus clearly too large. For the same reason it cannot be due to labelled C316 either. Helix 4 does contain one cysteine, C167, which is however embedded in the hydrophobic transmembrane bundle[30] and is not accessible to the charged and bulky label under the mild reaction conditions employed.[45] We therefore interpret the weaker difference density as due to a combination of errors: the Fourier difference approximation, the series termination error and the experimental errors in the structure factor amplitudes.

The strategy to localize single cysteine residues by site-directed heavy-atom labelling may be continued with other cysteine residues introduced by site-directed mutagenesis at strategic positions. Although the first 3D X-ray structure of rhodopsin is now available, several amino acid residues of the third cytoplasmic loop and the C-terminal tail have not yet been resolved. Furthermore, high crystallographic temperature factors observed for many other residues on the cytoplasmic surface indicate either a high flexibility of the loops or a disorder of the loop region in the 3D crystal.[30] Since these regions are of special interest for understanding the interaction with the G protein and/or the phosphorylation reactions regulating the receptor activity, it is instructive to compare the structural constraints obtained under different experimental conditions. 3D X-ray diffraction experiments were performed with crystals frozen in liquid nitrogen under cryogenic conditions (e.g. 100 K).[29] In addition, the crystal contacts may lead to additional loop-loop interactions, which are absent in the native membrane and 2D crystals. In cryo-electron microscopy, 2D crystals are embedded in vitrified ice and imaged at liquid nitrogen temperature in a high vacuum.[9] Our experiments are carried out at room temperature and 100 % relative humidity with a water layer between the crystalline membranes. Thus temperature effects, dehydration in the vacuum and loop-loop interactions, all of which may interfere with the loop structure, are minimal or absent in our experiments.

Since the heavy-atom position can be determined with an accuracy greater than the resolution of the X-ray diffraction patterns, our approach can significantly advance the interpretation of an electron density map. The C^{α} atom of the labelled cysteine residue can be localized within 4.1 Å of the heavy-atom. This would be sufficient to correlate regions of density in the structural map with the amino acid sequence. Furthermore, structural constraints from heavy-atom labelling can be used to improve the refinement of a membrane protein structure. Analysis of selectively labelled native residues or well-chosen cysteine mutants could provide valuable positional constraints for assigning and orienting transmembrane segments and loop domains.

Therefore our approach is of special interest for studies of other integral membrane proteins for which low-resolution structures from electron crystallography are available.

This approach is also very attractive for studying structural changes associated with different conformational states of a membrane protein. In rhodopsin, structural changes have been proposed by different methods including spin-labelling[51–53] and chemical cross-linking.[54] Since light-activation seems to destroy the available 3D crystals of rhodopsin[29], 2D crystals, where lattice contacts occur only in the transmembrane domain, might be more suitable to investigate the structural rearrangements. The structure of the cytoplasmic loop domain, which is crucial to G protein activation, has not yet been resolved by electron crystallography. If rhodopsin photointermediates could be trapped in 2D crystals, our approach may be used to characterize conformational changes by specific labelling at strategic sites.

Material and Methods

Retinas were isolated from fresh bovine eyes or were purchased from Lawson & Co, Lincoln, Nebraska. Lauryldimethylamine oxide and PCMB were purchased from Fluka. Cholesterol was purchased from Sigma. Copper-rhodium electron microscopy grids were from Graticules, Ltd (UK). Trespaphan support film was from Hoechst.

Isolation, purification and crystallisation of rhodopsin

ROS membranes were isolated at low ionic strength and purified on a stepwise sucrose density gradient.[55] Rhodopsin was purified by concanavalin A chromatography after solubilisation of the ROS membranes in lauryldimethylamine oxide (LDAO) as described.[9,56,57] 2D crystals were obtained after dialysis of the partially delipidated rhodopsin at 18 °C against a buffer containing 20 mM Hepes, 100 mM NaCl, 10 mM $MgCl_2$ and 3 mM NaN_3 (pH 7.0) for 11 days.[9] Additionally, DTT, mercaptoethanol and small volumes of organic solvents like isopropanol, MPD and DMSO were added to the dialysis buffer at varying concentrations. Native lipids were extracted from ROS membranes as described by Wiegand and Anderson[58]. If native lipids and/or cholesterol were used in reconstitution experiments, the required amount of lipids was dissolved in 1 ml chloroform and dried under a stream of argon. The lipids were dissolved in 1 ml diethylether, dried again under argon and finally dissolved in dialysis buffer containing 1 % (w/v) LDAO. 1 mg rhodopsin was then incubated at varying molar ratios between rhodopsin and lipids in dialysis buffer containing 0.5 % (w/v) LDAO at room temperature for two hours prior to dialysis.

Absorption spectroscopy and heavy-atom labelling

UV/VIS absorption spectra were recorded on a Shimadzu UV-2102PC spectrophotometer equipped with an integrating sphere. Rhodopsin 2D crystals were derivatized with PCMB with some modifications as described.[32] Prior to the labelling reaction, crystals were washed three times in labelling buffer (1 mM sodium phosphate, 20 mM NaCl, pH 7.0) and finally resuspended in labelling buffer at a concentration of 15-20 μM rhodopsin. The labelling was performed with a tenfold molar excess of PCMB in the dark at room temperature. After six hours, the unbound PCMB was removed by washing the crystals extensively in labelling buffer. The labelling stoichiometry was determined from the absorption difference between the labelled and unlabelled sample using the equation:

$$\mathrm{cMB/cRho} = \varepsilon(\mathrm{Rho}) \times \Delta A(\mathrm{MB})/A(\mathrm{Rho}) \times \Delta\varepsilon(\mathrm{MB}) \quad (2)$$

where cMB and cRho correspond to the molar concentrations of the bound mercuribenzoate and rhodopsin, respectively. A(Rho) is the absorbance of the retinal chromophore at 498 nm ($\varepsilon(\mathrm{Rho}) = 40{,}600\ \mathrm{M^{-1}\ cm^{-1}}$).[59] ΔA(MB) is the absorbance difference of the mercaptide at 240 nm ($\Delta\varepsilon(\mathrm{MB}) = 20{,}700\ \mathrm{M^{-1}\ cm^{-1}}$).[33]

Electron microscopy and image processing

5 μl of a crystal suspension were put on a carbon-coated glow-discharged electron microscopy grid and stained with 1 % (w/v) uranyl acetate without additional washing steps. Overview pictures were taken at low magnification using a Philips CM12 or Philips 420 electron microscope at 120 kV with a 50 μm condenser aperture as described.[2,26] For cryo-electron microscopy work, crystalline samples were put on a carbon-coated grid. After two minutes, excess liquid was blotted for ten seconds in a humidity chamber and the grid was frozen rapidly in liquid ethane.[9,60] Images were taken at liquid nitrogen temperature using a 200 kV Hitachi field emission microscope with a 30 μm condenser aperture and a GATAN cold stage (Gatan Ltd, Corby, UK). Electron micrographs were recorded under low-dose conditions (10-15 electrons/Å^2) at 60,000× magnification using a spot scan procedure.[61] All micrographs were recorded on Kodak SO-163 film and developed in full-strength D19 developer for 12 minutes at 20 °C.

Micrographs were screened by optical diffraction to identify crystalline arrays. Selected areas of 42 mm × 42 mm were scanned using a Zeiss SCAI densitometer (integration time 2.0 ms, step size 7 μm) and processed using the MRC image processing software.[62–64] Lattice distortions were removed using an interactive three-step unbending procedure as described.[9,63] Phases were corrected for effects of the contrast transfer function (CTF) against the recently obtained projection structure of rhodopsin.[9] The space group of the lattices was examined with the program ALLSPACE.[65] A reference data set of amplitudes and phases was obtained by combining four crystalline areas. After refinement of the phase origin and beam tilt (program ORIGTILTD), amplitudes were averaged (program AVRGAMPHS) and scaled (program SCALIMAMP3D) using bacteriorhodopsin as a reference. The scaling restores the typical resolution-dependent fall-off of amplitudes found by image processing compared to amplitudes obtained by electron diffraction and has been discussed in detail.[10,25,26] Projection density maps were calculated using the CCP4 crystallographic programs.[66]

X-ray diffraction experiments and data analysis

Labelled and unlabelled 2D crystals (0.7-1 mg rhodopsin) were centrifuged and each pellet was resuspended in 20-30 μl sodium phosphate buffer (pH 7.0) containing

0-20 mM NaCl. Oriented multilamellar films of 2D crystals were prepared by slowly drying a drop of the concentrated suspension on a thin Trespaphan support at a constant relative humidity near 100 %. When the drop became flat, another drop was applied on the top of it. The sample film finally covered an area of approximately 5 mm in diameter. X-ray diffraction measurements were performed using a rotating anode X-ray generator (Eliott-Marconi GX21) at 1.542 Å as described.[67] The oriented stacks of 2D crystals were mounted perpendicular to the X-ray beam in a chamber that was kept at 100 % relative humidity. In-plane powder diffraction patterns were recorded with a one-dimensional position-sensitive detector system (Braun OED-50-M) in the radial direction. To reduce the scattering of the primary beam in air, a helium chamber was placed between the sample and the detector. X-ray data were collected for 20-30 hours in one hour runs. All manipulations of the sample and the X-ray measurements were performed at room temperature under dim red light. All operations on the labelled and unlabelled samples were performed in parallel in order to avoid differences in the diffraction patterns due to differences in sample treatment.

X-ray data from individual one hour runs were carefully checked for systematic errors and changes of the background scattering due to changes of the ordering of the crystal stacks. Individual one hour runs were summed up to one spectrum for the labelled and unlabelled samples, respectively. Background subtraction was performed by fitting a 7 or 8 degree polynomial to the raw data.[33,35] The integrated intensities of the Bragg reflections were calculated by fitting a sum of Gaussian distributions to the data and corrected by a Lorentz factor of $(b^2h^2/a^2 + k^2)^{1/2}$. Intensities were then normalized to the sum of all intensities of a data set for the labelled and unlabelled sample, respectively. Fourier synthesis and Fourier difference maps were calculated using the experimental structure factors and the phases from electron microscopy. The justification of this procedure has been discussed in detail.[31] The label positions were then refined using the program Shelx 76.

Acknowledgements

We are grateful to Harald Otto and Wolfgang Behrens for their help and advice during the initial stages of this project. This research was supported, in parts, by grants from the BMBF (03-HE5FUB) and the DFG (Sfb 449) to M.P.H. T.M. was financially supported by a stipendium from the Nafög Kommission (FU Berlin). We also thank Norbert Krauss for his help with the refinement procedure.

References

1. Walz, T. & Grigorieff, N. (1998). Electron crystallography of two-dimensional crystals of membrane proteins. *J. Struct. Biol.* **121**, 142-161.
2. Schertler, G. F. X. (1999). Electron-crystallographic analysis of two-dimensional rhodopsin crystals. In *Structure-function Analysis of G Protein-coupled Receptors* (Wess, J., ed.), pp. 233-287, Wiley-Liss, Inc., New York.
3. Tsukihara, T. & Aoyama, H. (2000). Membrane protein assemblies - towards atomic resolution analysis. *Curr. Opin. Struct. Biol.* **10**, 208-212.
4. Kühlbrandt, W., Wang, D. N. & Fujiyoshi, Y. (1994). Atomic model of plant light-harvesting complex by electron crystallography. *Nature,* **367**, 614-621.
5. Grigorieff, N., Ceska, T. A., Downing, K. H., Baldwin, J. M. & Henderson, R. (1996). Electron-crystallographic refinement of the structure of bacteriorhodopsin. *J. Mol. Biol.* **259**, 393-421.
6. Mitsuoka, K., Hirai, T., Murata, K., Miyazawa, A., Kidera, A., Kimura, Y. & Fujiyoshi, Y. (1999). The structure of bacteriorhodopsin at 3.0 Å resolution based on electron crystallography: implication of the charge distribution. *J. Mol. Biol.* **286**, 861-882.
7. Murata, K., Mitsuoka, K., Hirai, T., Walz, T., Agre, P., Heymann, J. B. *et al*. (2000). Structural determinants of water permeation through aquaporin-1. *Nature,* **407**, 599-605.
8. Unger, V. M., Hargrave, P. A., Baldwin, J. M. & Schertler, G. F. X. (1997). Arrangement of rhodopsin transmembrane α-helices. *Nature,* **389**, 203-206.
9. Krebs, A., Villa, C., Edwards, P. C. & Schertler, G. F. X. (1998). Characterisation of an improved two-dimensional $p22_12_1$ crystal from bovine rhodopsin. *J. Mol. Biol.* **282**, 991-1003.
10. Havelka, W. A., Henderson, R. & Oesterhelt, D. (1995). Three-dimensional structure of halorhodopsin at 7 Å resolution. *J. Mol. Biol.* **247**, 726-738.
11. Auer, M., Scarborough, G. A. & Kühlbrandt, W. (1998). Three-dimensional map of the plasma membrane H^+-ATPase in the open conformation. *Nature,* **392**, 840-843.
12. Zhang, P. J., Toyoshima, C., Yonekura, K., Green, N. M. & Stokes, D. L. (1998). Structure of the calcium pump from sarcoplasmatic reticulum at 8 Å resolution. *Nature,* **392**, 835-839.
13. Williams, K. A., Geldermacher-Kaufer, U., Padan, E., Schuldiner, S. & Kühlbrandt, W. (1999). Projection structure of NhaA, a secondary transporter from *Escherichia coli*, at 4.0 Å resolution. *EMBO J.* **18**, 3558-3563.
14. Williams, K. A. (2000). Three-dimensional structure of the ion-coupled transporter protein NhaA. *Nature,* **403**, 112-115.
15. Collinson, I., Breyton, C., Duong, F., Tziatzios, C., Schubert, D., Or, E. *et al*. (2001). Projection structure and oligomeric properties of a bacterial core protein translocase. *EMBO J.* **20**, 2462-2471.
16. Heymann, J. A. W., Sarker, R., Hirai, T., Shi, D., Milne, J. L. S., Maloney, P. C. & Subramaniam, S. (2001). Projection structure and molecular architecture of OxIT, a bacterial membrane transporter. *EMBO J.* **20**, 4408-4413.
17. Mindell, J. A., Maduke, M., Miller, C. & Grigorieff, N. (2001). Projection structure of a ClC-type chloride channel at 6.5 Å resolution. *Nature,* **409**, 219-223.
18. Tate, C. G., Kunji, E. R. S., Lebendiker, M. & Schuldiner, S. (2001). The projection structure of EmrE, a proton-linked multidrug transporter from *Escherichia coli*, at 7 Å resolution. *EMBO J.* **20**, 77-81.
19. Strader, C. D., Fong, T. M., Graziano, M. P. & Tota, M. R. (1995). The family of G-protein-coupled receptors. *FASEB J.* **9**, 745-754.
20. Bockaert, J. & Pin, J. P. (1999). Molecular tinkering of G protein-coupled receptors: an evolutionary success. *EMBO J.* **18**, 1723-1729.
21. Ballesteros, J. A., Shi, L. & Javitch, J. A. (2001). Structural mimicry in G protein-coupled receptors: Implications of the high-resolution structure of rhodopsin for structure-function analysis of rhodopsin-like receptors. *Mol. Pharmacol.* **60**, 1-19.

22. Hargrave, P. A. & McDowell, J. H. (1992). Rhodopsin and phototransduction: a model system for G protein-linked receptors. *FASEB J.* **6**, 2323-2331.
23. Sakmar, T. P. (1998). Rhodopsin: a prototypical G protein-coupled receptor. *Prog. Nucl. Acid Res. Mol. Biol.* **59**, 1-34.
24. Menon, S. T., Han, M. & Sakmar, T. P. (2001). Rhodopsin: structural basis of molecular physiology. *Physiol. Rev.* **81**, 1659-1688.
25. Schertler, G. F. X., Villa, C. & Henderson, R. (1993). Projection structure of rhodopsin. *Nature,* **362**, 770-772.
26. Unger, V. M. & Schertler, G. F. X. (1995). Low resolution structure of bovine rhodopsin determined by electron cryo-microscopy. *Biophys. J.* **68**, 1776-1786.
27. Baldwin, J. M., Schertler, G. F. X. & Unger, V. M. (1997). An alpha-carbon template for the transmembrane helices in the rhodopsin family of G-protein-coupled receptors. *J. Mol. Biol.* **272**, 144-164.
28. Ruprecht, J., Mielke, T., Krebs, A. & Schertler, G. F. X. (2001). Electron crystallographic studies of rhodopsin. *Phase Transitions,* **In the press**.
29. Okada, T., Le Trong, I., Fox, B. A., Behnke, C. A., Stenkamp, R. E. & Palczewski, K. (2000). X-ray diffraction analysis of three-dimensional crystals of bovine rhodopsin obtained from mixed micelles. *J. Struct. Biol.* **130**, 73-80.
30. Palczewski, K., Kumasaka, T., Hori, T., Behnke, C. A., Motoshima, H., Fox, B. A. *et al*. (2000). Crystal structure of rhodopsin: a G protein-coupled receptor. *Science,* **289**, 739-745.
31. Plöhn, H. J. & Büldt, G. (1986). The determination of label positions in membrane proteins by neutron and anomalous X-ray diffraction of powder samples. *J. Appl. Crystallog.* **19**, 255-261.
32. Boyer, P. D. (1954). Spectrophotometric study of the reaction of protein sulfhydryl groups with organic mercurials. *J. Am. Chem. Soc.* **76**, 4331-4337.
33. Behrens, W., Alexiev, U., Mollaaghababa, R., Khorana, H. G. & Heyn, M. P. (1998). Structure of the interhelical loops and carboxyl terminus of bacteriorhodopsin by X-ray diffraction using site-directed heavy-atom labeling. *Biochemistry,* **37**, 10411-10419.
34. Glaeser, R. M., Baldwin, J., Ceska, T. A. & Henderson, R. (1986). Electron diffraction analysis of the M_{412} intermediate of bacteriorhodopsin. *Biophys. J.* **50**, 913-920.
35. Krebs, M. P., Behrens, W., Mollaaghababa, R., Khorana, H. G. & Heyn, M. P. (1993). X-ray diffraction of a cysteine-containing bacteriorhodopsin mutant and its mercury derivative. Localization of an amino acid residue in the loop of an integral membrane protein. *Biochemistry,* **32**, 12830-12834.
36. Seiff, F., Wallat, I., Ermann, P. & Heyn, M. P. (1985). A neutron diffraction study on the location of the polyene chain of retinal in bacteriorhodopsin. *Proc. Natl Acad. Sci. USA,* **82**, 3227-3231.
37. Heyn, M. P., Westerhausen, J., Wallat, I. & Seiff, F. (1988). High-sensitivity neutron diffraction of membranes: location of the Schiff base end of the chromophore of bacteriorhodopsin. *Proc. Natl Acad. Sci. USA,* **85**, 2146-2150.
38. Hauss, T., Grzesiek, S., Otto, H., Westerhausen, J. & Heyn, M. P. (1990). Transmembrane location of retinal in bacteriorhodopsin by neutron diffraction. *Biochemistry,* **29**, 4904-4913.
39. Behrens, W., Otto, H., Stuhrmann, H. B. & Heyn, M. P. (1998). Sulfur distribution in bacteriorhodopsin from multiple wavelength anomalous diffraction near the sulfur K-edge with synchrotron X-ray radiation. *Biophys. J.* **75**, 255-263.
40. Schertler, G. F. X. & Hargrave, P. A. (1995). Projection structure of frog rhodopsin in two crystal forms. *Proc. Natl Acad. Sci. USA,* **92**, 11578-11582.
41. Hasler, L., Heymann, J. B. & Engel, A. (1998). 2D crystallization of membrane proteins: rationales and examples. *J. Struct. Biol.* **121**, 162-171.
42. Warne, A., Wang, D. N. & Saraste, M. (1995). Purification and two-dimensional crystallization of bacterial cytochrome oxidases. *Eur. J. Biochem.* **234**, 443-451.
43. Albert, A. D., Young, J. E. & Yeagle, P. L. (1996). Rhodopsin-cholesterol interactions in bovine rod outer segment disk membranes. *Biochim. Biophys. Acta,* **1285**, 47-55.
44. Fliesler, S. J. & Anderson, R. E. (1982). Chemistry and metabolism of lipids in the vertebrate retina. *Prog. Lipid. Res.* **22**, 79-131.
45. De Grip, W. J., Bonting, S. L. & Daemen, F. J. M. (1975). Biochemical aspects of the visual process XXVIII. Classification of sulfhydryl groups in rhodopsin and other photoreceptor membrane proteins. *Biochim. Biophys. Acta,* **396**, 104-115.
46. Chen, Y. S. & Hubbell, W. L. (1978). Reactions of the sulfhydryl groups of membrane-bound bovine rhodopsin. *Membrane Biochem.* **1**, 107-130.
47. Findlay, J. B. C., Barclay, P. L., Brett, M., Davison, M., Pappin, D. J. C. & Thompson, P. (1984). The structure of mammalian rod opsins. *Vision Res.* **24**, 1501-1508.
48. Farahbakhsh, Z. T., Hideg, K. & Hubbell, W. L. (1993). Photoactivated conformational changes in rhodopsin: a time-resolved spin label study. *Science,* **262**, 1416-1419.
49. Imamoto, Y., Kataoka, M., Tokunaga, F. & Palczewski, K. (2000). Light-induced conformational changes of rhodopsin probed by fluorescent Alexa594 immobilized on the cytoplasmic surface. *Biochemistry,* **39**, 15225-15233.
50. Ceska, T. A. & Henderson, R. (1990). Analysis of high-resolution electron diffraction patterns from purple membrane labelled with heavy-atoms. *J. Mol. Biol.* **213**, 539-560.
51. Resek, J. F., Farahbakhsh, Z. T., Hubbell, W. L. & Khorana, H. G. (1993). Formation of the meta II photointermediate is accompanied by conformational changes in the cytoplasmic surface of rhodopsin. *Biochemistry,* **32**, 12025-12032.
52. Farrens, D. L., Altenbach, C., Yang, K., Hubbell, W. L. & Khorana, H. G. (1996). Requirement of rigid-body motion of transmembrane helices for light activation of rhodopsin. *Science,* **274**, 768-770.
53. Yang, K., Farrens, D. L., Altenbach, C., Farahbakhsh, Z. T., Hubbell, W. L. & Khorana, H. G. (1996). Structure and function in rhodopsin. Cysteines 65 and 316 are in proximity in a rhodopsin mutant as indicated by disulfide formation and interactions between attached spin labels. *Biochemistry,* **35**, 14040-14046.
54. Sheikh, S. P., Zvyaga, T. A., Lichtarge, O., Sakmar, T. P. & Bourne, H. R. (1996). Rhodopsin activation blocked by metal-ion-binding sites linking transmembrane helices C and F. *Nature,* **383**, 347-350.
55. McDowell, J. H. & Kühn, H. (1977). Light-induced phosphorylation of rhodopsin in cattle photoreceptor membranes: substrate activation and inactivation. *Biochemistry,* **16**, 4054-4060.

56. De Grip, W. J. (1982). Purification of bovine rhodopsin over concanavalin A-sepharose. *Methods Enzymol.* **81**, 197-207.
57. Schertler, G. F. X. & Hargrave, P. A. (2000). Preparation and analysis of two-dimensional crystals of rhodopsin. *Methods Enzymol.* **315**, 91-107.
58. Wiegand, R. D. & Anderson, R. E. (1982). Determination of molecular species of rod outer segment phospholipids. *Methods Enzymol.* **81**, 297-304.
59. Lin, S. W. & Sakmar, T. P. (1996). Specific tryptophan UV-absorbance changes are probes of the transition of rhodopsin to its active state. *Biochemistry,* **35**, 11149-11159.
60. Henderson, R., Baldwin, J. M., Ceska, T. A., Zemlin, F., Beckmann, E. & Downing, K. H. (1990). Model for the structure of bacteriorhodopsin based on high-resolution electron cryo-microscopy. *J. Mol. Biol.* **213**, 899-929.
61. Bullough, P. A. & Henderson, R. (1987). Use of spot scan procedure for recording low-dose micrographs of beam sensitive specimens. *Ultramicroscopy,* **21**, 223-230.
62. Amos, L. A., Henderson, R. & Unwin, P. N. T. (1982). Three-dimensional structure determination by electron microscopy of two-dimensional crystals. *Prog. Biophys. Mol. Biol.* **39**, 183-231.
63. Henderson, R., Baldwin, J. M., Downing, K. H., Lepault, J. & Zemlin, F. (1986). Structure of purple membrane from *Halobacterium halobium*: recording, measurement and evaluation of electron micrographs at 3.5 Å resolution. *Ultramicroscopy,* **19**, 147-178.
64. Crowther, R. A., Henderson, R. & Smith, J. M. (1996). MRC image processing programs. *J. Struct. Biol.* **116**, 9-16.
65. Valpuesta, J. M., Carrascosa, J. L. & Henderson, R. (1994). Analysis of electron microscope images and electron diffraction pattern of thin crystals of ϕ29 connectors in ice. *J. Mol. Biol.* **240**, 281-.
66. Collaborative Computational Project Number 4. (1994). The CCP4 Suite: programs for protein crystallography. *Acta Crystallog. sect. D,* **50**, 760-763.
67. Heyn, M. P., Dudda, C., Otto, H., Seiff, F. & Wallat, I. (1989). The purple to blue transition of bacteriorhodopsin is accompanied by a loss of the hexagonal lattice and a conformational change. *Biochemistry,* **28**, 9166-9172.

Edited by W. Baumeister

(Received 10 July 2001; received in revised form 22 November 2001; accepted 17 December 2001)